Full length article

On the impact of nanometric γ' precipitates on the tensile deformation of superelastic $Co_{49}Ni_{21}Ga_{30}$

A. Reul [a,*], C. Lauhoff [b], P. Krooß [b], C. Somsen [c], D. Langenkämper [c], M.J. Gutmann [d], B. Pedersen [e], M. Hofmann [e], W.M. Gan [f], I. Kireeva [g], Y.I. Chumlyakov [g], G. Eggeler [c], T. Niendorf [b], W.W. Schmahl [a]

[a] Department of Earth and Environmental Sciences, Applied Crystallography, Ludwig Maximilian University of Munich, Munich 80333, Germany
[b] Institute of Materials Engineering, University of Kassel, Kassel 34125, Germany
[c] Institute for Materials, Ruhr-University Bochum, Bochum 44801, Germany
[d] Rutherford Appleton Laboratory, ISIS Facility, Chilton Didcot, Oxfordshire OX11 0QX, United Kingdom
[e] Heinz Maier-Leibnitz Zentrum (MLZ), Technical University of Munich, Garching 85748, Germany
[f] German Engineering Materials Science Center (GEM) at MLZ, Helmholtz-Zentrum Hereon, Garching 85748, Germany
[g] Siberian Physical Technical Institute, Tomsk State University, Novosobornay Square 1, Tomsk 634050, Russian Federation

ARTICLE INFO

ABSTRACT

Results are presented reporting on the martensite domain variant selection and stress-induced martensite morphology in [001]-oriented superelastic $Co_{49}Ni_{21}Ga_{30}$ shape memory alloy (SMA) single crystals under tensile load. *In situ* neutron diffraction, as well as *in situ* optical- and confocal laser scanning microscopy were conducted focusing on three differently treated samples, i.e. in the as-grown, solution-annealed and aged condition. An aging treatment performed at 350 °C promotes the precipitation of nanoprecipitates. These second phase precipitates contribute to an increase of the number of habit plane interfaces, while reducing lamellar martensite plate thickness compared to the as-grown and solution-annealed (precipitate free) samples. During tensile loading, all samples show a stress-induced formation of martensite, characterized by one single domain variant ("detwinned") and one set of parallel habit planes in a shear band. The results clearly show that γ' nanoprecipitates do not necessarily promote multi-variant interaction during tensile loading. Thus, reduced recoverability in Co-Ni-Ga SMAs upon aging cannot be solely attributed to this kind of interaction as has been proposed in literature so far.

© 2022 Acta Materialia Inc. Published by Elsevier Ltd. All rights reserved.

1. Introduction

Since decades considerable efforts have been spent on the development of novel shape memory alloys (SMAs) and, specifically, high-temperature shape memory alloys (HT-SMAs) for numerous envisaged applications, e.g. as actuators and damping devices in various industries [1–3]. The unique functional properties of SMAs, i.e. shape memory effect (SME) and superelasticity (SE), rely on a fully reversible thermoelastic transformation from an austenitic high-temperature parent phase to a martensitic low-temperature product phase. Key criteria for high-temperature applicability above 100 °C are long term microstructural and functional stability and high resistance against plastic deformation [2,3]. Currently, the most widely employed SMA is binary Ni-Ti (also referred to as Nitinol, NiTi), characterized by excellent func-

tional properties and good biocompatibility [1,3–6]. However, the operation of NiTi is limited to about 75 °C, due to thermal instabilities and slip deformation at higher temperatures [5,7]. In this regard, precipitation hardening has been applied to reduce plastic deformation and improve functional properties. Additionally, ternary Ni-Ti-X alloys ($X =$ Zr, Hf, Au, Pt, Pd) have been designed to increase the transformation temperatures [3–5]. However, the demand for high amounts of noble metals (Au, Pt, Pd) is associated with high production costs. Currently, Ni-Ti-Hf HT-SMAs impart remarkable functional properties exceeding transformation temperatures of 400 °C [5]. However, alloying NiTi with refractory elements (Zr, Hf) causes limited workability due to pronounced brittleness. Thus, alternative alloy systems such as Cu-based, Ti-Ta-based and Ni-Al have been introduced as possible HT-SMA candidates [3]. Unfortunately, several drawbacks limit their commercial use in high-temperature applications. In particular, thermal instabilities and activation of slip remain challenging eventually promoting functional degradation impeding the transformation recoverability [3,5,8].

---

* Corresponding author.
E-mail address: alexander.reul@lrz.uni-muenchen.de (A. Reul).

In a series of studies, Heusler-type Co-Ni-Ga SMAs turned out to be promising alternatives for applications at elevated temperatures due to improved formability by controlled ductile γ-phase formation (disordered fcc) within the β-phase matrix and relatively inexpensive alloying elements [9–11]. A large SE response with a fully reversible stress-induced martensitic transformation up to 500 °C and excellent long-term cyclic stability without any kind of functional degradation up to 100 °C have been shown in single crystalline material [12,13] qualifying Co-Ni-Ga for high-temperature damping. In addition, appropriate heat treatment procedures have been shown to open up new possibilities for actuator applications at elevated temperatures by aging in the stress-induced martensite (SIM) phase, referred to as SIM-aging. As pointed out by [14,15] SIM-aging brought an increase of the transformation temperatures by about 150 °C as well as a fully reversible martensitic transformation upon thermo-mechanical cycling. As dislocation slip is suppressed in the {110} (001) slip system, most of the work on Co-Ni-Ga focused on single crystals in [001] orientation in order to study the fundamental mechanisms in this alloy system. Co-Ni-Ga single crystals in [001] orientation reveal large maximum SE strains of −4.6 and 8.6% in compression and tension, respectively, as well as excellent functional properties as compared to single crystals of other orientations or polycrystals [15–20]. In particular, polycrystalline Co-Ni-Ga alloys, which are crucially needed for the envisaged applications, often suffer from intergranular fracture upon thermomechanical processing and loading due to the pronounced anisotropic transformation behavior [16,20,21]. However, substantial progress has been made very recently in terms of both the establishment of robust processing routes and functional performance. Via hot extrusion [22,23] and additive manufacturing [24,25] microstructures characterized by minimal grain constraints have been introduced featuring high damage tolerance and good functional properties.

Beside segregation of the ductile γ-phase, in Co-Ni-Ga SMAs nanometric γ' precipitates (ordered fcc with $L1_2$ structure) can be introduced in the austenitic β-phase with intermediate-temperature aging treatments. Precipitation-hardening is a common approach in SMA systems to improve the functional properties at elevated temperatures, in particular, to obtain high-temperature SE, since the strength of the austenitic matrix is increased, eventually hampering plastic deformation and dislocation slip [3,6,8]. As pointed out by [11,26–30], γ' precipitates are effective in order to increase the hardness of the austenite and strongly affect the functional properties with respect to SME and SE in Co-Ni-Ga SMAs. However, the martensitic microstructure is substantially modified by the presence and morphology (spheroidal or elongated) of the γ' precipitates [28,30]. For instance, a notable twin-thickness reduction in thermally induced martensite has been observed with increasing particle size. This was related to both, pronounced elastic energy accumulation and difficulties in accommodating the transformation strain around the irregular stress fields of the non-transforming γ' precipitates [27]. As a consequence, martensite formation only took place in between large elongated γ' precipitates. Here, martensite concomitantly showed internal micromodulations (nano-twinning), finally causing inferior functional properties (reduction of transformation temperatures and strains, increase of transformation hysteresis) in relation to a condition featuring smaller (spheroidal) γ' precipitates [27,28]. Furthermore, oriented γ' precipitates with elongated shape (as a result of an aging treatment under superimposed stress) turned out to suppress nano-twinning and improve the accommodation of martensite compared to conditions with non-oriented γ' precipitates [28]. In a recent paper [29], the authors demonstrated that spheroidal γ' precipitates stimulate the evolution of a complex multi-variant microstructure of the stress-induced martensite under compressive loading. In contrast to a single, inter-

nally twinned martensite structure being present in both, as-grown [31] and solution-annealed [29] (precipitate-free) [001]-oriented single crystals, the coherency stress fields existing around the γ' precipitates were assumed to strongly promote the formation of further martensite variants upon stress-induced martensitic transformation under compression [29]. In particular, heat treatments (aging time and temperature) strongly affect the cyclic degradation resistance in [001]-oriented Co-Ni-Ga single crystals under compression loading. As pointed out by [30] large precipitates promote irreversibility, while small spheroidal precipitates with sizes up to 10 nm are associated with excellent functional stability.

In [001]-oriented Co-Ni-Ga single crystals under tensile loading the formation of a multi-variant microstructure is supposed to be suppressed as pointed out by theoretical calculations [17] and experimental results [13,19,31]. However, up to now, no studies are available discussing the role of the morphology and variant selection of stress-induced martensite under tensile loading. Thus, in the present study microstructural analysis has been conducted using *in situ* optical microscopy (OM) as well as *in situ* neutron diffraction at different stages of SE experiments. Neutron diffraction is a valuable method for phase quantification and assessment of structural information from bulk samples, since neutrons exhibit a large penetration depth [29,33–35]. Focusing on [001]-oriented Co-Ni-Ga single crystals in solution-annealed, precipitation-hardened and as-grown (being the most studied state in literature) [13,16,31,32,34–38] condition, a thorough understanding of the stress-induced martensitic transformation is established. This, in turn, will contribute to a solid understanding of the complex interrelationships between microstructure, martensitic transformation (MT) and functional properties in Heusler-type Co-Ni-Ga alloys and other SMAs being characterized by similar characteristics.

2. Experimental

2.1. Sample preparation

Large single crystals with a nominal composition of $Co_{49}Ni_{21}Ga_{30}$ (at%) were grown using the Bridgeman technique in a helium environment. Flat dog-bone tensile samples with a gauge length of 18 mm and a cross section of 1.5 x 1.5 mm² were obtained by electro-discharge machining (EDM) from the bulk single crystals such that the loading axis was parallel to the [001] crystal direction of the austenitic phase. All samples were mechanically ground in order to remove the EDM affected surface layer. Tensile samples were tested in as-grown, solution-annealed and aged condition. In order to obtain a single-phase condition free of any secondary phases [27–29], solution-annealing was conducted in quartz glass tubes under argon atmosphere at 1200 °C for 12 h followed by breaking of the quartz tubes and air cooling to room temperature. Aging of the solution-annealed sample to form nanometric γ' precipitates ($\approx$ 5 nm size) with spheroidal shape [29] was performed at 350 °C for 1 h under ambient atmosphere.

2.2. In situ optical microscopy (OM)

Quasi-static uniaxial tensile experiments were performed at 100 °C at a nominal strain rate of 10^{-3} s^{-1} on a servohydraulic load frame in displacement control with a fixed nominal strain of 11% upon loading and a minimum stress of 50 N for unloading. The SE response of $Co_{49}Ni_{21}Ga_{30}$ single crystals was evaluated in single cycle tensile tests. Nominal strain was calculated from displacement data. The selected test temperature of 100 °C ensured a fully austenitic state for all sample conditions prior to SE testing allowing for meaningful comparison with data of previous work [29]. *In*
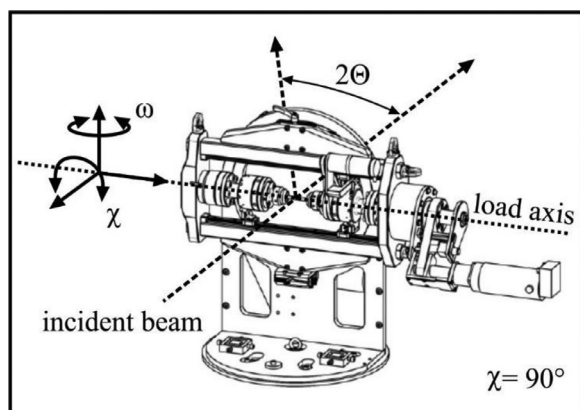
Fig. 1. Schematic view of the rotatable tensile rig in the horizontal set-up. The orientation between the incident beam and the load axis is given by the angles ω and χ (modified after [41]).

situ OM analysis of the transforming samples was conducted at selected load stages of the SE stress-strain hysteresis to characterize SIM morphology. In addition to the mechanical grinding using silicon carbide down to 5 μm grit size, the side surfaces being investigated were mechanically polished using a colloidal SiO_2 polishing suspension with 0.02 μm particle size. Grinding and polishing were performed in the austenitic condition. Surface images were collected within a representative area using a digital microscope. Furthermore, high resolution confocal laser scanning microscopy (CLSM) was employed on the aged sample using a higher magnification to assess SIM morphology. The CLSM equipped with a 408 nm violet laser has a maximum axial and lateral resolution of 10 nm and 120 nm, respectively.

2.3. In situ neutron diffraction

In situ neutron diffraction focusing on a tensile sample in the as-grown condition was carried out under the same conditions as in case of the *in situ* OM experiments using the STRESS-SPEC diffractometer at FRMII, Munich. *In situ* neutron diffraction was carried out to assess SIM domain variant selection at selected and pre-defined load levels of the SE stress-strain curve. Diffraction patterns were recorded at a scattering angle of $2\Theta = 56°$ using a wavelength of 1.352 Å. The orientation of the load axis with respect to the incident beam was $\chi = 0°$ (load axis vertical to the scattering plane) and $\chi = 90°$ (load axis in the scattering plane, Fig. 1). At each loading stage, rocking scan measurements were performed in 0.1° steps at a fixed ω-orientation (orientation of the main sample table with respect to the incident beam) around $\omega \pm 1.5°$ (10 s data collection for each step). The software package Stress Texture Calculator (SteCa) was used for data extraction [39]. The method applied for analysis is based on a single peak fitting routine to extract peak positions and integral intensities. For further details on the setup of STRESS-SPEC the reader is referred to [40,41].

In addition, *in situ* neutron diffraction was carried out using the single crystal diffractometer SXD at ISIS neutron source, Rutherford Appleton Laboratory, Oxfordshire. Uniaxial tensile tests were performed focusing on the solution-annealed and the subsequently aged sample (i.e. the same sample before and after aging) under the same conditions as in the *in situ* OM experiments. Diffraction patterns were recorded on six equatorial detectors for each pre-defined load level in the austenitic and martensitic state for 30 and 90 min, respectively. Diffraction data were indexed and integrated using the software package SXD2001 [42]. The refinement of the identified Bragg peak positions relies on optimization of the match

between observed and calculated peak positions. Then, peak intensities are determined based on the refined peak positions using a single peak fitting routine as a function of time-of-flight. For further details on the setup of SXD, the reader is referred to [42]. In addition, consecutive steps of data analysis are detailed in the *Supplementary Material*.

3. Results

In previous investigations [28–30], the SE response of $Co_{49}Ni_{21}Ga_{30}$ single crystals containing nanometric γ' precipitates showed a significantly increased stress hysteresis width ($\Delta\sigma$, as defined in the inset in Fig. 2) compared to solution-annealed and as-grown material [32] in compression. The increased stress-hysteresis was rationalized based on the increased frictional energy impeding habit plane motion when γ' precipitates are present [29,30]. The open question remained whether this friction is caused by (i) triggering of microstructures with multiple domains and multiple orientations of habit planes by the γ' precipitates as observed under compression [29] or (ii) direct interaction of γ' precipitates with the moving austenite-martensite phase boundary. To tackle this prevailing research gap, in the present work *in situ* experiments using neutron diffraction and optical microscopy were performed focusing on the SE response of $Co_{49}Ni_{21}Ga_{30}$ single crystals under tensile loads for three material states (Fig. 2): a) as-grown, b) solution-annealed and c) aged, i.e. only the latter containing well-defined γ' precipitates.

3.1. Co-Ni-Ga (as-grown)

Fig. 2a shows the single cycle tensile SE response at 100 °C of the [001]-oriented $Co_{49}Ni_{21}Ga_{30}$ single crystalline sample in the as-grown condition. The stress-strain curve is characterized by a narrow stress hysteresis $\Delta\sigma$ of 11 MPa, a low critical stress for the onset of stress-induced martensitic transformation σ_{crit} of about 140 MPa and a plateau-type character. This excellent SE behavior with a fully reversible MT is in good agreement with data already reported for as-grown $Co_{49}Ni_{21}Ga_{30}$ single crystals [13].

Fig. 3a shows diffraction patterns for the as-grown tensile sample collected at nine load stages on the stress-plateau (region II), where the load axis was oriented vertical and perpendicular to the scattering plane ($\chi = 0°$). For the sake of brevity, only diffraction data for four out of nine diffraction patterns are displayed for the forward transformation. The experiment in $\chi = 0°$ orientation was performed in the range of 2.5 to 9.3% strain. As revealed by the diffraction pattern (Fig. 3a), a single martensite domain variant V_3 (Bain-correspondent variant BCV_3 out of the three possible BCVs, see Fig. 3c and text below) is formed at the beginning of the stress-plateau at 2.8% strain. The corresponding diffraction peak in region II arises from the (200) lattice plane of domain variant V_3. Upon further loading to 8.5% strain the volume fractions of austenitic and martensitic phase decreased and increased, respectively, as can be deduced from the peak intensities in Fig. 3a. At the end of the stress-strain plateau, i.e. at 9.3% macroscopically applied tensile strain, the volume fraction of austenite and SIM is 0 and 100%, respectively. Furthermore, with the load axis oriented in the scattering plane ($\chi = 90°$), diffraction patterns were collected at seven load stages during the forward transformation in the elastic austenite region I (not shown) and another seven load stages up to 11% strain in the elastic martensite region III (Fig. 3b). The diffraction patterns (Fig. 3b) reveal the presence of the single martensite domain variant (002) V_3 throughout region III as well. The corresponding diffraction peaks in region III arise from the (002) lattice plane of domain variant V_3. Furthermore, constant diffraction intensities from the (002) lattice plane indicate a constant volume fraction of this single martensite domain variant
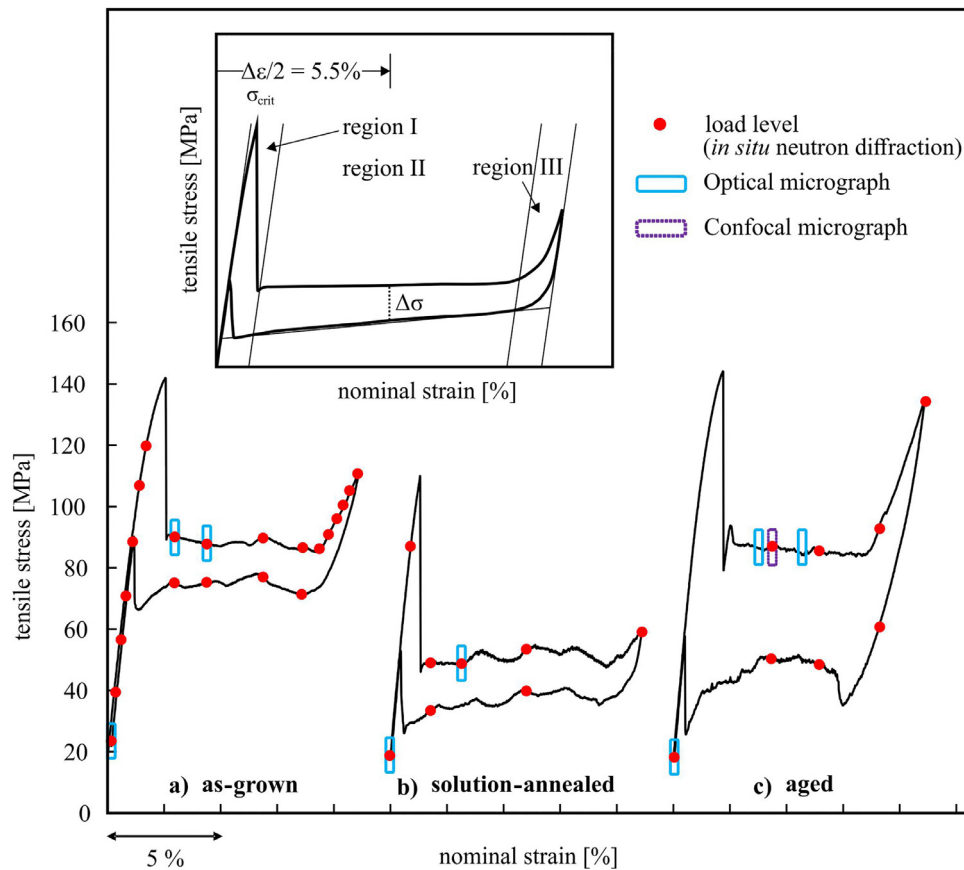
Fig. 2. Superelastic stress-strain responses under tensile load at 100 °C of [001]-oriented $Co_{49}Ni_{21}Ga_{30}$ single crystals in the as-grown (a), solution-annealed (b) and aged (c) condition. The stress hysteresis, $\Delta\sigma$, was measured at half of the applied nominal strain amplitude $\Delta\varepsilon/2$. σ_{crit} is the critical transformation stress level for the onset of stress-induced forward transformation. The elastic austenite region, stress-plateau and elastic martensite region are referred to as region I, region II and region III, respectively. The red dots highlight the load levels considered for assessment of the experimental results of neutron diffraction data. The blue and purple rectangles indicate where optical and confocal micrographs, respectively, were taken. (For interpretation of the references to color in this figure legend, the reader is referred to the web version of this article.)

(highlighted by the inset depicting data for three out of seven load stages in Fig. 3b).

Fig. 3c schematically highlights the formation of a correspondent variant pair (CVP) based on the Bain-correspondence variants (BCVs). In the cubic to tetragonal transformation three possible Bain-correspondence variants BCV_1, BCV_2 and BCV_3 (BCV_1 is not shown) evolve, each with the four-fold axis (c-axis) along one of the cubic austenite axes. Martensite domain variant orientations are derived from the stress-free intergrowth of two BCVs. This necessitates a rotation of the domain variants in relation to the initial orientation of the BCVs. Correspondingly, twinning of the pairs BCV_3/BCV_2, BCV_3/BCV_1 and BCV_2/BCV_1 is possible along a stress-free twin plane of the type {110}. In the present case, the corresponding domain variants V_2 and V_3 shown in Fig. 3c form a CVP. The occurrence of twinned martensite would be revealed by the appearance of two pairs of Bragg-peaks on the corresponding diffraction patterns, i.e. $(200)V_3/(002)V_2$ and $(200)V_2/(002)V_3$ with the load axis vertical to the scattering plane ($\chi = 0°$) and in the scattering plane ($\chi = 90°$), respectively (Fig. 3c). Thus, in case of twinned martensite additional diffraction signals would have been detected from $(002)V_2$ and $(200)V_2$ lattice planes at $2\Theta = 50.5°$ (Fig. 3a) and $2\Theta = 59.5°$ (Fig. 3b), respectively. However, the obtained diffraction patterns do not indicate such additional domain variants on the stress-plateau (Fig. 3a) and in the elastic martensite region (Fig. 3b). Hence, fully detwinned SIM was observed up to 11% strain comprising only V_3 (BCV_3), i.e. BCV_1 and BCV_2, where the extensional c-axis is oriented perpendicular to the [001] tensile load direction, are suppressed.

Optical micrographs were recorded at specific load levels of the stress-strain curve (cf. blue markers in Fig. 2a). Fig. 4 shows corresponding microstructures of the as-grown [001]-oriented $Co_{49}Ni_{21}Ga_{30}$ tensile sample, already probed in the neutron diffraction experiment, at 2.8% (b) and 4.4% (c,d) applied strain during forward transformation. The loading direction and reference austenitic microstructure of the sample recorded prior to mechanical testing in the load free condition are displayed in Fig. 4a. The forward transformation (Fig. 4b) is characterized by the formation of a single dominant martensite plate (bottom, V_3) and a shear band with lamellar microstructural features comprising a set of a few well-defined parallel interface boundaries between the untransformed austenite (marked as A in Fig. 4b) and martensite. The direct interfaces between the austenitic matrix and martensite, which can be distinguished by the optical contrast, are known as habit planes (HP). As revealed by *in situ* neutron diffraction (Fig. 3a), the dominant martensite plate and the lamellar martensite plates (martensite lamellae) between the arrangement of parallel HPs forming a shear band comprise only a single martensite domain variant (V_3). Upon further loading to 4.4% strain, the martensitic transformation proceeds with the growth of the dominant martensite plate and the movement of the shear band as depicted in Fig. 4c. The SIM morphology is highlighted by the optical micrograph recorded at higher magnification (Fig. 4d).

3.2. Co-Ni-Ga (solution-annealed)

Fig. 2b shows the tensile SE response at 100 °C of the [001]-oriented $Co_{49}Ni_{21}Ga_{30}$ single crystalline sample in the solution-
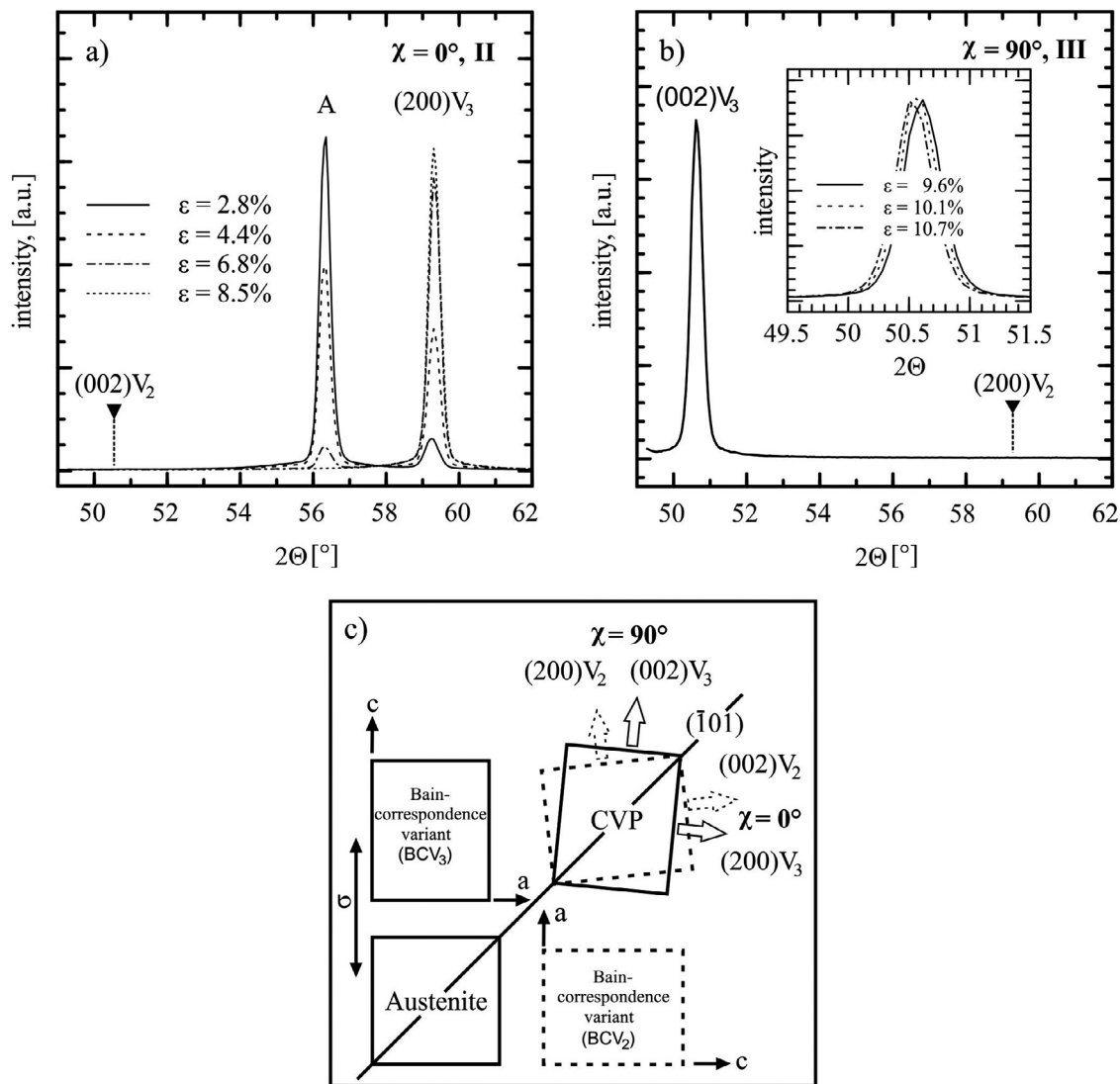
Fig. 3. *In situ* neutron diffraction patterns of a [001]-oriented $Co_{49}Ni_{21}Ga_{30}$ single crystal in the as-grown condition indicating the phase state on the stress-plateau (a) and elastic martensite region (b). Note, the orientation of the load axis with respect to the incident beam is $\chi = 0°$ (vertical to the scattering plane, (a)) and $\chi = 90°$ (load axis in the scattering plane, (b)). The schematic (c) illustrates the formation of a correspondent variant pair (CVP) based on the Bain-correspondence variants (BCVs). The CVP comprises domain variant V_2 (dashed rectangle, which is not observed for the present direction of stress) and V_3 (bold rectangle).

annealed condition. The SE behavior is characterized by a narrow stress hysteresis width $\Delta\sigma$ of 11 MPa, a low critical transformation stress σ_{crit} of about 110 MPa and a plateau-type character. These SE characteristics and the fully reversible MT are in good agreement with data already reported for solution-annealed $Co_{49}Ni_{21}Ga_{30}$ single crystals [17,19].

Diffraction data (see chapter 2.3 and the *Supplementary Material* for details on data acquisition and assessment) of the solution-annealed tensile sample were recorded at nine load levels up to 11% nominal strain (cf. Figs. 2b and 5). For the sake of brevity, only diffraction data for four out of nine diffraction patterns are displayed for the forward transformation. Diffraction intensities show that the solution-annealed sample only comprises a single domain variant V_3 of SIM on the stress-plateau (region II, 3 and 6% in Fig. 5) and within the elastic martensite region (region III, 11% in Fig. 5). As can be deduced from the diffraction intensities, the volume fraction of the single domain variant V_3 is almost 100% at maximum applied strain.

Beforehand, *in situ* OM was performed on the same sample used in the neutron diffraction experiment to assess SIM morphology. Note, as the neutron diffraction experiment revealed the for-

mation of one single domain variant during loading and unloading, only one representative optical micrograph is shown for the forward transformation. Micrographs were recorded at the marked positions of the stress-strain curve in Fig. 2b for the reference austenitic microstructure in the unloaded state and at 2.8% strain upon loading (Fig. 6a and b, respectively). The optical micrograph of the solution-annealed tensile sample recorded at 2.8% strain reveals a single dominant martensite plate consisting of domain variant V_3 and non-transformed austenite A (Fig. 6b). Noteworthy, the shear band is a region of one well-defined martensite lamella and a single habit plane (HP).
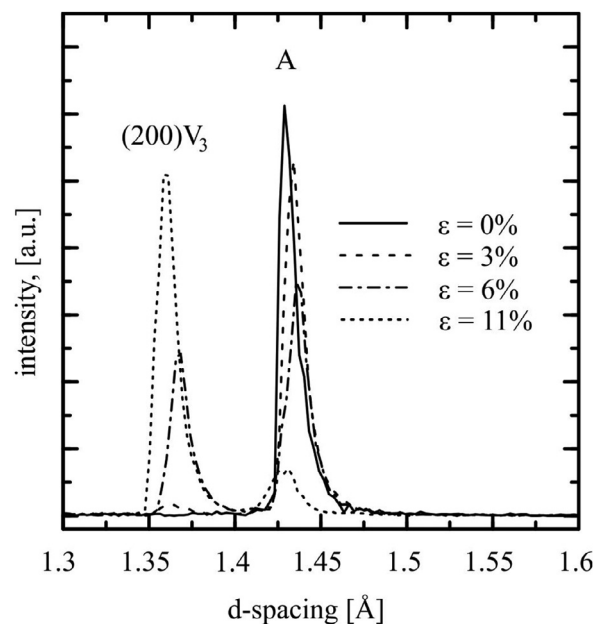
3.3. Co-Ni-Ga (aged)

Fig. 2c shows the tensile SE response at 100 °C of the [001]-oriented $Co_{49}Ni_{21}Ga_{30}$ single crystalline sample after aging at 350 °C for 1 h. The segregation of γ' precipitates causes significant differences in the stress-strain response in comparison to the as-grown and solution-annealed material states, in particular with respect to $\Delta\sigma$. The SE response is characterized by a fully reversible MT, a plateau-type character and a critical transformation stress
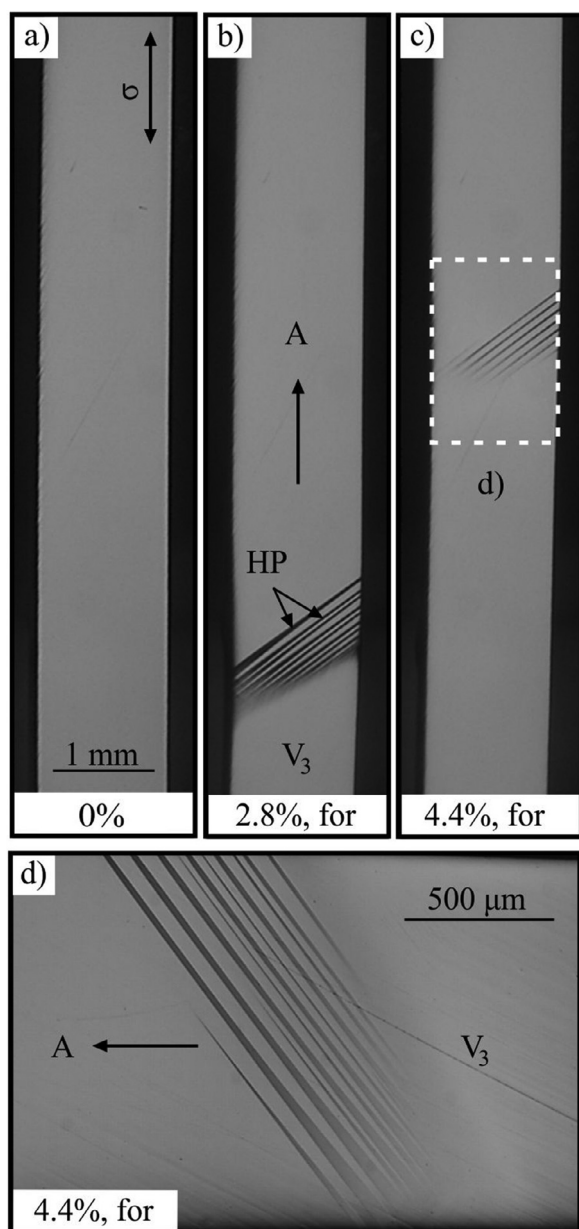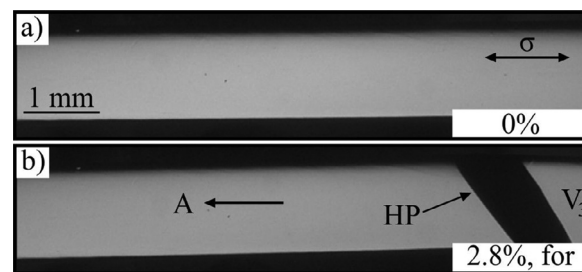
Fig. 4. *In situ* optical micrographs recorded under tensile load at 100 °C for the as-grown [001]-oriented Co$_{49}$Ni$_{21}$Ga$_{30}$ single crystal (the same sample studied by neutron diffraction, Fig. 3). Loading direction (for subimages (a) to (c)) is marked in the upper right corner of (a). The microstructure of the SIM at higher magnification is depicted in (d) (here loading direction is horizontal). The optical contrasts within the shear band are due to alternating austenite/martensite lamellae separated by habit plane (HP) interfaces. A: austenite, V$_3$: martensite, for: forward transformation.

Fig. 5. Diffraction intensity as a function of d-spacing obtained at different macroscopically applied tensile strains for the [001]-oriented Co$_{49}$Ni$_{21}$Ga$_{30}$ single crystal in the solution-annealed condition. Only a single martensite domain variant V$_3$ is present throughout the whole transformation plateau up to 11% strain.

Fig. 6. *In situ* optical micrographs for the solution-annealed [001]-oriented Co$_{49}$Ni$_{21}$Ga$_{30}$ single crystal (the same sample investigated by neutron diffraction in Fig. 5) under tensile load at 100 °C. The micrographs were recorded at the marked positions of the stress-strain curve in (Fig. 2b) in the unloaded state and at 2.8% strain upon loading. The loading direction is displayed in the upper right corner of image (a). A: austenite, V$_3$: martensite, HP: habit plane, for: forward transformation.

σ_{crit} of about 140 MPa. However, the stress hysteresis width $\Delta\sigma$ of 35 MPa is considerably increased (by a factor of about 3).

In a previous study [29] it was shown that aging at 350 °C for 1 h leads to the formation of finely dispersed γ' precipitates. However, it is important to mention that γ' nanoprecipitates are not detectable using neutron diffraction. This fact is attributed to coherently scattering regions of γ' precipitates confined to finite extensions in the order of 5 nm. This strongly reduces long-range order over which translational periodicity is present [43]. Consequently, when the three dimensionally periodic atomic structure is present on a short length scale the precision of TOF is significantly reduced and does not result in well-defined Bragg peaks. Accordingly, γ' nanoprecipitates are not resolvable via neutron

diffraction, but are detectable using high-resolution transmission electron microscopy (HRTEM). The HRTEM image (Fig. 7, recompiled from [29]) shows spheroidal γ' precipitates with sizes up to 5 nm. The selected area electron diffraction (SAED) pattern (inset in Fig. 7) obtained from the [001]$_{B2}$ zone axis reveals sharp and clear superlattice reflection spots at h+k+l= 2n indicating B2-type (space group P m -3̄ m) chemical ordering in the system. In addition, very weak superlattice spots can be observed in the center of diffuse streaks connecting the strong Bragg spots of austenite along {110}$_{B2}$ directions in reciprocal space (marked by the white arrows). The weak superlattice ordering indicates the γ' phase [27] and is related to an fcc unit cell (space group F m -3 m). Clearly, the diffuse intensities are stronger towards the center of the reciprocal lattice than further outside. Thus, we suppose that the diffuse streaks can be attributed to antiphase domain walls related to the chemical (i.e. substitutional) order of the γ' phase, disturbing its long-range lattice periodicity. This is related to the spheroidal appearance of γ' phase-order clusters in real space.

Diffraction data (see chapter 2.3 and the *Supplementary Material* for details on data acquisition and assessment) of the aged tensile sample were recorded at nine load stages up to 11% nominal
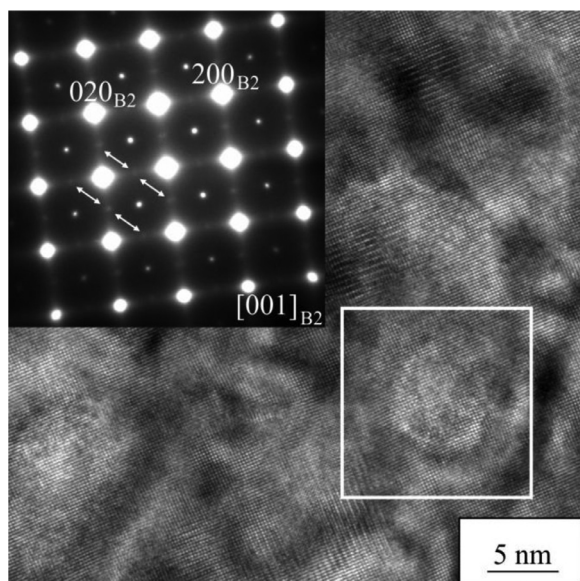
Fig. 7. HRTEM image of γ' precipitates formed after aging at 350 °C for 1 h. The spheroidal γ' precipitate within the white rectangle has a size of 5 nm. The inset shows the corresponding SAED pattern with diffuse superlattice reflection spots of the γ' phase marked by the white arrows (recompiled from [29]).
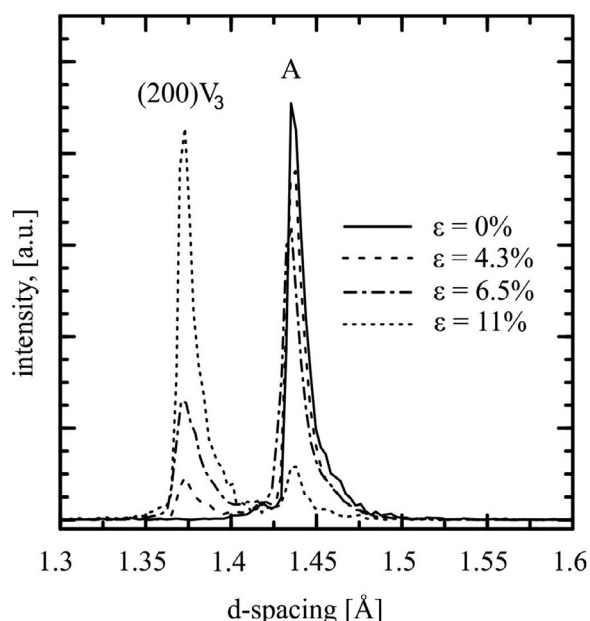
Fig. 8. Diffraction intensity as a function of d-spacing obtained at different macroscopically applied tensile strains for the [001]-oriented $Co_{49}Ni_{21}Ga_{30}$ single crystal in the aged (1 h/350 °C) condition. Only a single martensite domain variant V_3 is present throughout the whole transformation plateau up to 11% strain.

strain (cf. Fig. 2c). For the sake of brevity, again, only diffraction data for four out of nine diffraction patterns are displayed for the forward transformation in Fig. 8. As revealed by the diffraction intensities, the aged sample comprises austenite and the single domain variant V_3 of the SIM on the stress-plateau (region II, 4.3 and 6.5% in Fig. 8) and the elastic martensite region (region III, 11% in Fig. 8). As can be deduced from the diffraction intensities, the volume fraction of the single domain variant V_3 is almost 100% at maximum applied strain.

The prevailing phase constitution for the three different material states was evaluated using in situ neutron diffraction. A direct comparison of the three different material states is given by

the lattice parameters (Table 1) which were experimentally determined on the stress-plateau at $\sim$ 6% applied macroscopic tensile strain. They indicate the relative magnitudes of the tetragonal lattice distortion. The spontaneous strain related to the austenite to martensite transition is positive in c-direction and negative in a-direction, while the c-axis strain is twice as high as the value of the a-axis strain. The c/a ratio is a measure for the unit cell tetragonality of the SIM directly obtained from lattice parameters. On the stress-plateau at 6 % macroscopic tensile strain in the aged sample the tetragonality is 1.1, i.e. significantly smaller than the ca. 1.16 in the as-grown and solution-annealed conditions. Accordingly, the lattice distortion of the single martensite domain variant at 6 % macroscopic tensile strain is smaller in the aged sample containing γ' nanoprecipitates compared to the as-grown and solution-annealed material state. This microscopic finding correlates well with the reduced macroscopic transformation strain when γ' nanoprecipitates are present. However, the relatively low macroscopic transformation strain is to be attributed not only to smaller lattice strains, but also to the reduction of transformable volume fraction of the material as the γ' nanoprecipitates are known to not transform upon loading [28]. To further shed light on the complex interplay between microstructure (lattice strain and nanoprecipitates) and transformation behavior additional experiments need to be conducted in follow up studies.

In situ OM was performed on the same sample used in the neutron diffraction experiment beforehand (cf. Fig. 8) to assess the SIM morphology in the presence of γ' precipitates as illustrated in Fig. 9. The optical micrographs were recorded at the marked positions of the stress-strain curve in Fig. 2c, i.e. in the unloaded state, at 3.6 and at 5.5% applied strain (see *Supplementary Material* for further micrographs recorded during reverse transformation). The shear band of the aged tensile sample is characterized by a reduction of martensite lamellar thickness and an increased number of parallel HPs during the forward transformation (Fig. 9b,c) in direct contrast to the very few well-defined HPs and the single HP seen in the as-grown and solution-annealed material states, respectively. The shear band depicted at 5.5% strain is highlighted by the optical micrograph recorded at higher magnification (Fig. 9d).

However, difficulties in the visualization of the prevailing martensite lamellae within the shear band are obvious (Fig. 9d). For clarity, a more detailed analysis of the SIM morphology within the shear band was conducted by *in situ* confocal laser scanning microscopy only in this condition. The micrograph shown in Fig. 10 was recorded at 4.2% strain during the forward transformation. Besides the obvious reduction of martensite lamellar thickness, the lamellae seem to be slightly distorted (Fig. 10) and they are not oriented to the same (well-defined) degree compared to the as-grown condition (cf. Fig. 4d).

4. Discussion

The aim of the present paper is to provide in-depth insights into the underlying microstructural mechanisms leading to the increased stress hysteresis width of $Co_{49}Ni_{21}Ga_{30}$ single crystals containing nanometric γ' precipitates ($\sim$ 5 nm size) as compared to solution-annealed and as-grown material. Previous investigations [27–29] concluded that an increased contribution of friction of the moving austenite-martensite phase boundary is caused by the γ' precipitates. It was assumed that this could be induced by two different reasons: (i) by triggering of microstructures with multiple domain variants of SIM and multiple orientations of HPs, which were observed under compressive load, eventually leading to pronounced interfacial (interphase and/or intervariant) interactions; (ii) by γ' precipitates acting as obstacles to the moving austenite-martensite phase boundary. In particular, the impact of γ' precipitates on SIM morphology and SE response under tensile loading

Table 1

Lattice parameters of austenite (B2) and stress-induced martensite (L1$_0$) for Co-Ni-Ga in the as-grown, solution-annealed and aged condition. Lattice parameters were measured at 100 °C in the unloaded state (austenite) and during forward transformation on the stress-plateau at ~6% applied tensile strain.

Sample state	Crystal structure	Lattice parameters (Å)				Tetragonality
		a	b	c	$\alpha = \beta = \gamma$	c/a
as-grown	L1$_0$: tetragonal	2.733(1)	2.733(1)	3.163(3)	90°	1.157(1)
	B2: cubic	2.874(4)			90°	
solution-annealed	L1$_0$: tetragonal	2.738(8)	2.738(8)	3.179(13)	90°	1.161(8)
	B2: cubic	2.868(5)			90°	
aged (1 h/350 °C)	L1$_0$: tetragonal	2.792(6)	2.792(6)	3.072(13)	90°	1.100(7)
	B2: cubic	2.873(5)			90°	

has not been addressed so far. To provide for novel insights, *in situ* techniques, i.e. neutron diffraction, OM and CSLM during isothermal single cycle mechanical tests were used to further characterize the effect of γ' precipitates in aged samples in comparison to the solution-annealed reference state, being free of any secondary phases, and the as-grown condition, which is the most studied material state in literature [13,16,31,32,34–38].

Based on theoretical calculations using the energy minimization theory [17], the formation of one martensite domain variant is favored in tension along the [001] axis. Bulk information obtained in the present study by *in situ* neutron diffraction revealed one single domain variant of SIM for all three investigated material conditions, being perfectly consistent with theory [17]. Thorough diffraction analysis of SIM in the as-grown condition demonstrated the presence of a single domain variant V$_3$ throughout the whole stress-plateau (region II, Fig. 3a) and the elastic martensite region (region III, Fig. 3b). Furthermore, intensities of domain variant V$_3$ remained constant within the entire elastic martensite region. Accordingly, the formation of alternative twin domains can be excluded indicating the presence of a fully detwinned microstructure during the whole transformation cycle. Such stress-induced martensite transformation (SIMT) behavior is also present after both solution-annealing and aging for 1 h at 350 °C, i.e. the thermal treatments conducted have virtually no influence on the martensite variant selection in [001]-oriented single crystals under tensile loading.

Interestingly, the presence of nanometric γ' precipitates following the aging treatment at 350 °C for 1 h does neither impose multiple domain variants of SIM nor HPs of multiple orientations with respect to the loading direction. As can be deduced from diffraction data shown in Fig. 8, domain variant selection in the aged [001]-oriented Co$_{49}$Ni$_{21}$Ga$_{30}$ single crystal does not change up to the maximum applied tensile strain of 11%. Under tensile load, the Bain-correspondence variant BCV$_3$ is favored by the external applied stress, whereas BCV$_1$ and BCV$_2$ are suppressed. In compression BCV$_1$ and BCV$_2$ are favored, while BCV$_3$ is suppressed [35]. Previous work [29,30] focusing on aged Co$_{49}$Ni$_{21}$Ga$_{30}$ under compressive loading demonstrated the occurrence of multiple domain variants comprising two sets of CVPs formed by BCV$_1$ and BCV$_2$. This phenomenon was attributed to strong coherency stress fields in the matrix due to the formation of small (spheroidal) γ' precipitates (cf. Fig. 7). It was derived that due to the stress fields introduced by the precipitates multi-domain variant microstructures emerge. This was in contrast to material being free of precipitates, where only a single internally twinned CVP formed under compression [29]. The evolution of strong local stress fields in the matrix due to the formation of small coherent or semi-coherent Ti$_3$Ni$_4$ precipitates has been already revealed in NiTi SMAs [44]. These local stress fields arise from the mismatch in lattice parameters between the Ti$_3$Ni$_4$ precipitates and the matrix. Eventually, this promotes locally resolved shear stress on the martensite CVPs
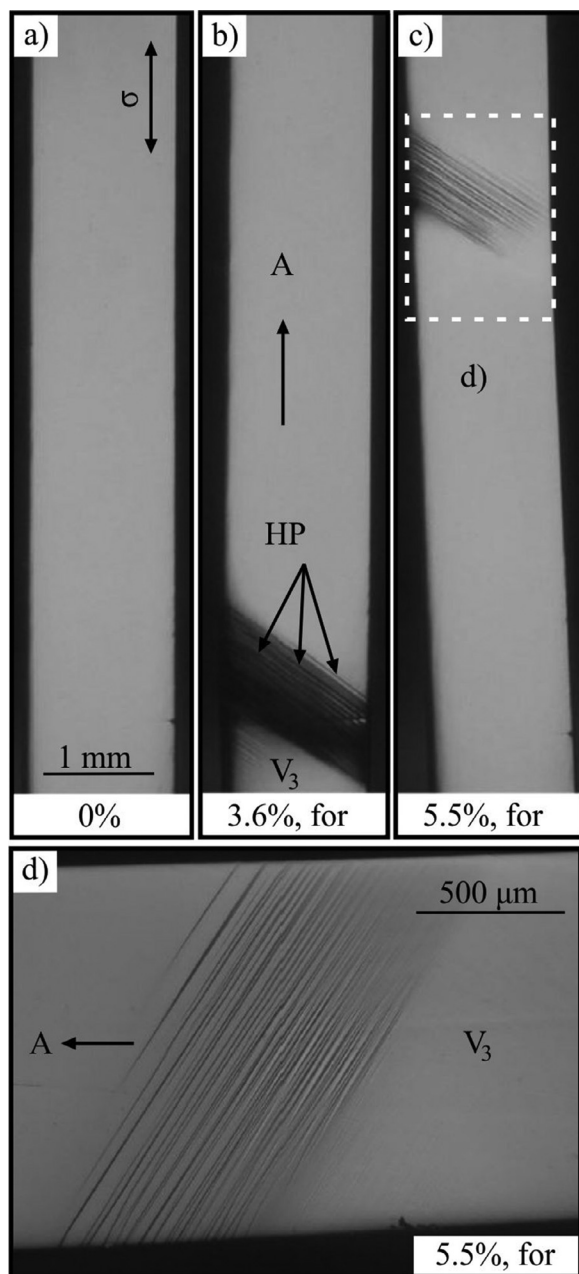
and the generation of preferential nucleation sites for martensite [44]. A similar behavior was expected for the aged tensile sample containing small coherent γ' precipitates ($\sim$ 5 nm). In tension, however, the strong local stress fields are not able to promote additional domain variants, as can be deduced from the corresponding diffraction pattern (Fig. 8). As a result, the formation of one single domain variant of martensite is favored under tensile load (despite the presence of nanometric coherent γ' precipitates), a behavior being fundamentally different to the compressive stress state [29].

Optical micrographs revealed significant differences in martensite morphology, in particular, with respect to the number and thickness of martensite lamellae in the shear band. In the as-grown condition the stress-induced phase transformation proceeds by the propagation of a dominant martensite plate and a shear band composed of martensite lamellae, which are arranged between a set of a few well-defined parallel HPs (Fig. 4b-d). In this material condition the nucleation of only few well-defined parallel HPs during the forward transformation is inferred from chemical inhomogeneities acting as preferential nucleation sites [32,45]. In solution-annealed Co$_{49}$Ni$_{21}$Ga$_{30}$ the SIMT from B2 to L1$_0$ is led by a dominant martensite plate and a well-defined shear band featuring only one martensite lamella, i.e. the transformation behavior is characterized by only a single austenite-martensite interface (Fig. 6), which is characteristic for single crystals with low defect density [46]. In turn, γ' precipitates with spheroidal shape obtained by an aging at 350 °C for 1 h (cf. Fig. 7) promote the reduction of the martensite lamellar thickness and, at the same time, lead to an increased number of HPs. The formation of partially transforming regions in the shear band is characterized by slightly distorted, more or less parallel HPs during the forward transformation (Fig. 10). This is in good agreement with the significant refinement of the martensitic morphology in thermally [27] and SIM (under compression [29]) reported for aged Co$_{49}$Ni$_{21}$Ga$_{30}$ single crystals. The refined microstructure was attributed to the elastic deformation of the non-transforming γ' precipitates and the surrounding matrix during MT, eventually leading to an increase in elastic energy accumulation and, thus, the reduction in martensite twin thickness [27].

In the present study focusing on tensile loading, the introduction of nanometric γ' precipitates strongly affects the SIM morphology and, eventually, promotes a substantially different stress-strain response in relation to the as-grown and solution-annealed (precipitate-free) material. As can be deduced from the stress-strain curves in Fig. 2, the stress hysteresis value $\Delta\sigma$ of 35 MPa in the aged condition is about 3 times higher than in the solution-annealed and as-grown conditions both characterized by a $\Delta\sigma$ of 11 MPa.
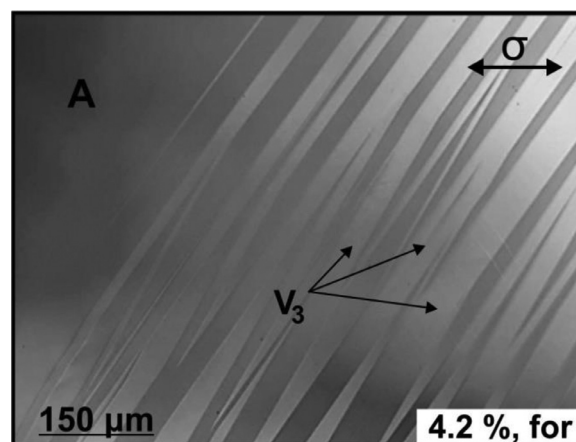
Findings can be rationalized based on consideration of well-known concepts proposed in literature. Commonly, the widening of the stress hysteresis $\Delta\sigma$ can be attributed to three general energy dissipative processes during the martensitic transforma-

Fig 10. Micrograph obtained by confocal laser scanning microscopy of the aged (1 h/350 °C) [001]-oriented $Co_{49}Ni_{21}Ga_{30}$ single crystal already shown in Figs. 8 and 9. The micrograph was recorded at the marked position of the stress-strain curve in Fig. 2c during the forward transformation at 4.2% strain. Loading direction is marked in the upper right corner. A: austenite, V_3: martensite, for: forward transformation.

Fig. 9. *In situ* optical micrographs of the aged (1 h/350 °C) [001]-oriented $Co_{49}Ni_{21}Ga_{30}$ single crystal (the same sample investigated by neutron diffraction in Fig. 8) under tensile load at 100 °C. The micrographs were recorded at the marked positions of the stress-strain curve in (Fig. 2c), i.e. in the unloaded state, at 3.6 and 5.5% strain. Loading direction for subimages (a) to (c) is marked in the upper right corner of (a). The microstructure of the SIM at higher magnification is depicted in (d) at 5.5% strain during the forward transformation (here loading direction is horizontal). A: austenite, V_3: martensite, HP: habit plane, for: forward transformation.

tion [8,17,28,45]. The first energy dissipative process is frictional work that is required for interface motion [46,47]. Here, the interface motion is controlled and hampered by interfacial (interphase and/or intervariant) and interface-precipitate interactions. Recent findings on Co-Ni-Ga [29] showed that γ' nanoprecipitates under compressive load impose a complex multi-variant martensite microstructure. Such a kind of microstructure has been characterized by two sets of differently oriented, parallel HP interfaces and multiple domain variants of SIM [29]. It was concluded that interfacial interactions contribute to the widening of the stress hysteresis most significantly. However, γ' nanoprecipitates in the aged tensile sample do not induce multi-variant microstructures (characterized by multiple orientations of HPs and multiple domain variants). Thus, such a kind of evolution cannot be exploited to rationalize the widening of the stress hysteresis in the aged $Co_{49}Ni_{21}Ga_{30}$ single crystal of the present study. Instead, another contributing factor has to be dealt with. The aged sample revealed a shear band characterized by numerous lamellar martensite plates within one set of parallel HPs, however, with only one single domain variant of SIM. As a consequence, the increase in frictional energy and its contribution to the widened stress hysteresis is mainly attributed to γ' nanoprecipitates acting as obstacles for the moving austenite-martensite phase boundaries.

The second dissipative process is attributed to the dissipation of stored elastic strain energy. Stored elastic strain energy is dissipated, when the coherency strains of austenite-martensite phase boundaries relax, eventually widening the stress hysteresis [46,47,53]. This dissipative process is primarily linked to localized plastic deformation induced by mechanical cycling in direct vicinity of incoherent precipitates. Dislocations, induced by the incoherent precipitate boundaries and inherited by the martensitic phase, are known to substantially increase the interfacial friction and, thus, significantly contribute to an additional irreversible component of the transformation, eventually increasing hysteresis width [47]. However, small precipitates were shown to remain coherent with the matrix even after mechanical cycling [8]. Hence, dissipation of stored elastic energy around coherent precipitates is thought to be much less effective due to the absence of severe dislocation activity [27]. However, it has to be emphasized at this point that crystallography of Ni-Ti including its ternary derivates (these alloys being most intensively studied in the field of SMAs) [5,8,48,49] and the Co-Ni-Ga system studied here are clearly different. The same holds true for novel Fe-based SMAs [50–52]. Thus, transferability of results and conclusions has to be further elaborated and critically assessed in comprehensive studies to be conducted in future research. Still, the relaxation of coherency strains at the austenite-martensite phase boundaries around coherent γ' precipitates, the major contributing mechanism reported for Ni-Ti [54], seems to be of minor importance for the increased size of the stress hysteresis in the aged tensile sample considered here.

The third dissipative process accounts for the dissipation of interfacial energy, i.e. solely takes into account the direct thermodynamic contribution of the interface itself. The formation of γ' precipitates comprises a change in the surface and phase bound-

ary energies, eventually affecting the macroscopic stress-strain response in terms of the stress hysteresis $\Delta\sigma$. Consequently, the reduction of martensite lamellar thickness and the increase in number of HPs (Fig. 9) jointly increase the interfacial energy contribution and, thus, lead to the widening of the stress hysteresis width $\Delta\sigma$ [28]. The small volume fraction of the shear band with respect to the entire sample volume clearly indicates very limited, however, detectable interfacial energy dissipation in the aged $Co_{49}Ni_{21}Ga_{30}$ tensile sample.

The narrow stress hysteresis $\Delta\sigma$ of 11 MPa in both the solution-annealed and as-grown condition is attributed to an easy propagation of the dominant martensite plate and the shear band due to minimal energy dissipation [17,45]. The aged sample, in contrast, clearly reveals that a larger stress hysteresis width is governed by nanometric γ' precipitates, which act as obstacles for phase boundary movement, while additional contributions to the stress hysteresis such as dissipation of elastic strain energy and interfacial energy play only a minor role (see discussion in the paragraphs above). It is worth noting that the introduction of small γ' precipitates ($\sim$ 5 nm sized) following an aging treatment at 350 °C for 1 h does not contribute to severe interfacial interactions under tensile loading. This fact can be deduced from the occurrence of only one domain variant (Fig. 8) in the dominant martensite plate and the shear band (Fig. 9). On the other hand, previous work on $Co_{49}Ni_{21}Ga_{30}$ single crystals under compression demonstrated that small γ' precipitates ($\sim$ 5 nm sized) trigger multi-variant martensite microstructures, i.e. multiple domains of SIM and multiple orientations of HPs [29,30]. Such kind of microstructures characterized by pronounced interfacial interactions contribute to pronounced dissipation of frictional energy during SIMT, which has been concluded to reduce transformation recoverability [13,32,52]. The present results indicate that aging treatments for Co-Ni-Ga SMAs are not necessarily associated with the formation of multi-variant martensite microstructures. It is supposed that the impact of γ' precipitates on the final functional properties in Co-Ni-Ga SMA single crystals is strongly dependent on their size and morphology [27,28].

5. Summary and conclusions

Tensile tests at 100 °C were conducted on as-grown, solution-annealed and aged $Co_{49}Ni_{21}Ga_{30}$ [001]-oriented single crystals. Detailed microstructural analysis of stress-induced martensite (SIM) was performed using *in situ* neutron diffraction and *in situ* optical- and confocal laser scanning microscopy (OM and CLSM, respectively). The main findings of the present work can be summarized as follows:

1. *In situ* neutron diffraction analysis revealed the presence of only one single domain variant of martensite ("fully detwinned") throughout the whole transformation cycle for all conditions, i.e. as-grown, solution-annealed and aged $Co_{49}Ni_{21}Ga_{30}$ single crystals in [001] orientation. Correspondingly, from three possible Bain-correspondence variants (BCVs) in the cubic to tetragonal transformation only BCV_3 with the c-axis parallel to the loading axis is favored. BCV_1 and BCV_2 with their c-axes transversal to the loading direction are suppressed.

2. *In situ* OM revealed substantial differences between the microstructure of SIM comparing the three investigated conditions. Spheroidal γ' precipitates in the aged material significantly reduce martensite lamellar thicknesses and increase the number of parallel habit planes (HPs) within a shear band. The solution-annealed condition shows yet a fundamentally different microstructure upon loading characterized by one dominant martensite plate and a shear band with one martensite lamella and a single HP.

3. All samples revealed a fully reversible superelastic (SE) response. However, γ' precipitates significantly increase the width of the stress hysteresis ($\Delta\sigma$) compared to the particle-free solution-annealed and as-grown conditions.

4. After formation of γ' precipitates still only one set of parallel HPs is seen, clearly indicating the absence of variant-variant interactions upon tensile loading in [001]-oriented Co-Ni-Ga single crystals. Most severely, interactions between the nanometric γ' precipitates and austenite-martensite phase boundaries lead to a significant increase of the stress hysteresis width.

Declaration of Competing Interest

The authors declare that they have no known competing financial interests or personal relationships that could have appeared to influence the work reported in this paper.

Supplementary materials

Supplementary material associated with this article can be found, in the online version, at doi:10.1016/j.actamat.2022.117835.

References

[1] K. Otsuka, C.M. Wayman, Shape Memory Materials, Cambridge University Press, Cambridge, 1999.

[2] D.C. Lagoudas, Shape Memory Alloys: Modeling and Engineering Applications, Springer, New York, 2008.

[3] J. Ma, I. Karaman, R.D. Noebe, High temperature shape memory alloys, Int. Mater. Rev. 55 (2010) 257–315.

[4] K. Otsuka, X. Ren, Physical metallurgy of Ti-Ni-based shape memory alloys, Prog. Mater. Sci. 50 (2005) 511–678.

[5] H. Sehitoglu, L. Patriarca, Y. Wu, Shape memory strains and temperatures in the extreme, Curr. Opin. Solid State Mater. Sci. 21 (2017) 113–120.

[6] S. Miyazaki, T. Imai, Y. Igo, K. Otsuka, Effect of cyclic deformation on the pseudoelasticity characteristics of Ti-Ni alloys, Metall. Trans. A Phys. Metall. Mater. Sci. 17 (1986) 115–120 A.

[7] H. Sehitoglu, I. Karaman, R. Anderson, X. Zhang, K. Gall, H.J. Maier, Y. Chumlyakov, Compressive response of NiTi single crystals, Acta Mater. 48 (2000) 3311–3326.

[8] K. Gall, H.J. Maier, Cyclic deformation mechanisms in precipitated NiTi shape memory alloys, Acta Mater. 50 (2002) 4643–4657.

[9] K. Oikawa, T. Ota, F. Gejima, T. Ohmori, R. Kainuma, K. Ishida, Phase equilibria and phase transformations in new B2-type ferromagnetic shape memory alloys of Co-Ni-Ga and Co-Ni-Al systems, Mater. Trans. 42 (2001) 2472–2475.

[10] J. Liu, H. Xie, Y. Huo, H. Zheng, J. Li, Microstructure evolution in CoNiGa shape memory alloys, J. Alloy. Compd. 420 (2006) 145–157.

[11] E. Dogan, I. Karaman, Y.I. Chumlyakov, Z.P. Luo, Microstructure and martensitic transformation characteristics of CoNiGa high temperature shape memory alloys, Acta Mater. 59 (2011) 1168–1183.

[12] J. Dadda, H.J. Maier, I. Karaman, Y.I. Chumlyakov, Cyclic deformation and austenite stabilization in $Co_{35}Ni_{35}Al_{30}$ single crystalline high-temperature shape memory alloys, Acta Mater. 57 (2009) 6123–6134.

[13] P. Krooß, T. Niendorf, P.M. Kadletz, C. Somsen, M.J. Gutmann, Y.I. Chumlyakov, W.W. Schmahl, G. Eggeler, H.J. Maier, Functional fatigue and tension–compression asymmetry in [001]-oriented $Co_{49}Ni_{21}Ga_{30}$ high-temperature shape memory alloy single crystals, Shape Mem. Superelasticity 1 (2015) 6–17.

[14] T. Niendorf, P. Krooß, C. Somsen, G. Eggeler, Y.I. Chumlyakov, H.J. Maier, Martensite aging - avenue to new high temperature shape memory alloys, Acta Mater. 89 (2015) 298–304.

[15] C. Lauhoff, P. Krooß, D. Langenkämper, C. Somsen, G. Eggeler, I. Kireeva, Y.I. Chumlyakov, T. Niendorf, Martensite aging in (0 0 1) -oriented $Co_{49}Ni_{21}Ga_{30}$ single crystals in tension, Funct. Mater. Lett. 11 (2018) 15–18.

[16] J. Dadda, H.J. Maier, D. Niklasch, I. Karaman, H.E. Karaca, Y.I. Chumlyakov, Pseudoelasticity and cyclic stability in $Co_{49}Ni_{21}Ga_{30}$ shape-memory alloy single crystals at ambient temperature, Metall. Mater. Trans. A 39 (2008) 2026–2039.

[17] J.A. Monroe, I. Karaman, H.E. Karaca, Y.I. Chumlyakov, H.J. Maier, High--temperature superelasticity and competing microstructural mechanisms in $Co_{49}Ni_{21}Ga_{30}$ shape memory alloy single crystals under tension, Scr. Mater. 62 (2010) 368–371.

[18] I.V. Kireeva, Y.I. Chumlyakov, Z.V. Pobedennaya, I.V. Kretinina, E. Cesari, S.B. Kustov, C. Picornell, J. Pons, I. Karaman, Orientation dependence of superelasticity in ferromagnetic single crystals $Co_{49}Ni_{21}Ga_{30}$, Phys. Met. Metallogr. 110 (2010) 78–90.

[19] T. Niendorf, J. Dadda, J. Lackmann, J.A. Monroe, I. Karaman, E. Panchenko, H.E. Karaca, H.J. Maier, Tension - compression asymmetry in $Co_{49}Ni_{21}Ga_{30}$ high-temperature shape memory alloy single crystals, Mater. Sci. Forum. 738–739 (2013) 82–86.

[20] M. Vollmer, P. Krooß, C. Segel, A. Weidner, A. Paulsen, J. Frenzel, M. Schaper, G. Eggeler, H.J. Maier, T. Niendorf, Damage evolution in pseudoelastic polycrystalline Co-Ni-Ga high-temperature shape memory alloys, J. Alloy. Compd. 633 (2015) 288–295.

[21] C. Lauhoff, M. Vollmer, P. Krooß, I. Kireeva, Y.I. Chumlyakov, T. Niendorf, Pathways towards grain boundary engineering for improved structural performance in polycrystalline Co–Ni–Ga shape memory alloys, Shape Mem. Superelasticity 5 (2019) 73–83.

[22] T. Niendorf, C. Lauhoff, E. Karsten, G. Gerstein, A. Liehr, P. Krooß, H.J. Maier, Direct microstructure design by hot extrusion – high-temperature shape memory alloys with bamboo-like microstructure, Scr. Mater. 162 (2019) 127–131.

[23] E. Karsten, G. Gerstein, O. Golovko, A. Dalinger, C. Lauhoff, P. Krooss, T. Niendorf, A. Samsonenko, H.J. Maier, Tailoring the microstructure in polycrystalline Co–Ni–Ga high-temperature shape memory alloys by hot extrusion, Shape Mem. Superelasticity 5 (2019) 84–94.

[24] C. Lauhoff, A. Fischer, C. Sobrero, A. Liehr, P. Krooß, F. Brenne, J. Richter, M. Kahlert, S. Böhm, T. Niendorf, Additive manufacturing of Co-Ni-Ga high--temperature shape memory alloy: processability and phase transformation behavior, Metall. Mater. Trans. A Phys. Metall. Mater. Sci 51 (2020) 1056–1061.

[25] C. Lauhoff, N. Sommer, M. Vollmer, G. Mienert, P. Krooß, S. Böhm, T. Niendorf, Excellent superelasticity in a Co-Ni-Ga high-temperature shape memory alloy processed by directed energy deposition, Mater. Res. Lett. 8 (2020) 314–320.

[26] I.V. Kireeva, Y.I. Chumlyakov, I.V. Kretinina, I. Karaman, E. Cesari, Superelasticity in CoNiGa single crystals containing γ-phase particles, Russ. Phys. J. 54 (2012) 1295–1297.

[27] I.V. Kireeva, J. Pons, C. Picornell, Y.I. Chumlyakov, E. Cesari, I.V. Kretinina, Influence of γ' nanometric particles on martensitic transformation and twinning structure of L10 martensite in Co-Ni-Ga ferromagnetic shape memory single crystals, Intermetallics 35 (2013) 60–66.

[28] I.V. Kireeva, C. Picornell, J. Pons, I.V. Kretinina, Y.I. Chumlyakov, E. Cesari, Effect of oriented γ' precipitates on shape memory effect and superelasticity in Co-Ni-Ga single crystals, Acta Mater. 68 (2014) 127–139.

[29] C. Lauhoff, A. Reul, D. Langenkämper, P. Krooß, C. Somsen, M.J. Gutmann, I. Kireeva, Y.I. Chumlyakov, W.W. Schmahl, T. Niendorf, Effect of nanometric γ'-particles on the stress-induced martensitic transformation in $\langle 001 \rangle$-oriented $Co_{49}Ni_{21}Ga_{30}$ shape memory alloy single crystals, Scr. Mater. 168 (2019) 42–46.

[30] C. Lauhoff, A. Reul, D. Langenkämper, P. Krooß, C. Somsen, M.J. Gutmann, B. Pedersen, I. Kireeva, Y.I. Chumlyakov, G. Eggeler, W.W. Schmahl, T. Niendorf, Effects of aging on the stress-induced martensitic transformation and cyclic superelastic properties in Co-Ni-Ga shape memory alloy single crystals under compression, Acta Mater. 226 (2022) 117623.

[31] P. Krooß, P.M. Kadletz, C. Somsen, M.J. Gutmann, Y.I. Chumlyakov, W.W. Schmahl, H.J. Maier, T. Niendorf, Cyclic degradation of $Co_{49}Ni_{21}Ga_{30}$ high-temperature shape memory alloy: on the roles of dislocation activity and chemical order, Shape Mem. Superelasticity 2 (2016) 37–49.

[32] J. Dadda, H.J. Maier, I. Karaman, Y. Chumlyakov, High-temperature *in-situ* microscopy during stress-induced phase transformations in $Co_{49}Ni_{21}Ga_{30}$ shape memory alloy single crystals, Int. J. Mater. Res. 101 (2010) 1503–1513.

[33] J. Khalil-Allafi, G. Eggeler, W.W. Schmahl, D. Sheptyakov, Quantitative phase analysis in microstructures which display multiple step martensitic transformations in Ni-rich NiTi shape memory alloys, Mater. Sci. Eng. A 438–440 (2006) 593–596.

[34] P.M. Kadletz, P. Krooß, Y.I. Chumlyakov, M.J. Gutmann, W.W. Schmahl, H.J. Maier, T. Niendorf, Martensite stabilization in shape memory alloys - experimental evidence for short-range ordering, Mater. Lett. 159 (2015) 16–19.

[35] A. Reul, C. Lauhoff, P. Krooß, M.J. Gutmann, P.M. Kadletz, Y.I. Chumlyakov, T. Niendorf, W.W. Schmahl, *In situ* neutron diffraction analyzing stress-induced phase transformation and martensite elasticity in [001]-oriented $Co_{49}Ni_{21}Ga_{30}$ shape memory alloy single crystals, Shape Mem. Superelasticity 4 (2018) 61–69.

[36] V.A. Chernenko, J. Pons, E. Cesari, I.K. Zasimchuk, Transformation behaviour and martensite stabilization in the ferromagnetic Co-Ni-Ga Heusler alloy, Scr. Mater. 50 (2004) 225–229.

[37] J. Dadda, H.J.J. Maier, I. Karaman, H.E.E. Karaca, Y.I.I. Chumlyakov, Pseudoelasticity at elevated temperatures in [001]oriented $Co_{49}Ni_{21}Ga_{30}$ single crystals under compression, Scr. Mater. 55 (2006) 663–666.

[38] V.A. Chernenko, S. Besseghini, E. Villa, A. Gambardella, J.I. Pérez-Landazabal, Elastic and superelastic properties of $Co_{49}Ni_{22}Ga_{29}$ single crystal, Appl. Phys. Lett. 90 (2007) 201914.

[39] C. Randau, U. Garbe, H.G. Brokmeier, StressTextureCalculator: a software tool to extract texture, strain and microstructure information from area-detector measurements, J. Appl. Crystallogr. 44 (2011) 641–646.

[40] M. Hofmann, R. Schneider, G.A. Seidl, J. Rebelo-Kornmeier, R.C. Wimpory, U. Garbe, H.G. Brokmeier, The new materials science diffractometer STRESS-SPEC at FRM-II, Phys. B Condens. Matter. 385–386 (2006) 1035–1037.

[41] M. Hoelzel, W.M. Gan, M. Hofmann, C. Randau, G. Seidl, P. Jüttner, W.W. Schmahl, Rotatable multifunctional load frames for neutron diffractometers at FRM II - Design, specifications and applications, Nucl. Instrum. Methods Phys. Res. Sect. A Accel. Spectrometers Detect. Assoc. Equip. 711 (2013) 101–105.

[42] D.A. Keen, M.J. Gutmann, C.C. Wilson, SXD - the single-crystal diffractometer at the ISIS spallation neutron source, J. Appl. Crystallogr. 39 (2006) 714–722.

[43] V.K. Pecharsky, P.Y. Zavalij, Fundamentals of Powder Diffraction and Structural Characterization of Materials, Springer, 2009.

[44] K. Gall, H. Sehitoglu, Y.I. Chumlyakov, I.V. Kireeva, H.J. Maier, The influence of aging on critical transformation stress levels and martensite start temperatures in NiTi: part I- aged microstructure and micro-mechanical modeling, J. Eng. Mater. Technol. Trans. ASME. 121 (1999) 19–27.

[45] Y.I. Chumlyakov, I.V. Kireeva, E.Y. Panchenko, V.A. Kirillov, E.E. Timofeeva, I.V. Kretinina, Y.N. Danil'son, I. Karaman, H. Maier, E. Cesari, Thermoelastic martensitic transformations in single crystals with disperse particles, Russ. Phys. J. 54 (2012) 937–950.

[46] R.J. Salzbrenner, M. Cohen, On the thermodynamics of thermoelastic martensitic transformations, Acta Metall. 27 (1979) 739–748.

[47] G.B. Olson, M. Cohen, Thermoelastic behavior in martensitic transformations, Scr. Metall. 9 (1975) 1247–1254.

[48] G.S. Bigelow, S.A. Padula, A. Garg, D. Gaydosh, R.D. Noebe, Characterization of ternary NiTiPd high-temperature shape-memory alloys under load-biased thermal cycling, Metall. Mater. Trans. A Phys. Metall. Mater. Sci. 41 (2010) 3065–3079.

[49] O. Benafan, G.S. Bigelow, A. Garg, R.D. Noebe, Viable low temperature shape memory alloys based on Ni-Ti-Hf formulations, Scr. Mater. 164 (2019) 115–120.

[50] Y. Tanaka, Y. Himuro, R. Kainuma, Y. Sutou, T. Omori, K. Ishida, Ferrous polycrystalline shape-memory alloy showing huge superelasticity, Science 327 (80) (2010) 1488–1490.

[51] J. Ma, B.C. Hornbuckle, I. Karaman, G.B. Thompson, Z.P. Luo, Y.I. Chumlyakov, The effect of nanoprecipitates on the superelastic properties of FeNiCoAlTa shape memory alloy single crystals, Acta Mater. 61 (2013) 3445–3455.

[52] P. Krooß, C. Somsen, T. Niendorf, M. Schaper, I. Karaman, Y. Chumlyakov, G. Eggeler, H.J. Maier, Cyclic degradation mechanisms in aged FeNiCoAlTa shape memory single crystals, Acta Mater. 79 (2014) 126–137.

[53] E. Hornbogen, The effect of variables on martensitic transformation temperatures, Acta Metall. 33 (1985) 595–601.

[54] R.F. Hamilton, H. Sehitoglu, Y. Chumlyakov, H.J. Maier, Stress dependence of the hysteresis in single crystal NiTi alloys, Acta Mater. 52 (2004) 3383–3402.